31st Joint Propulsion Conference, San Diego, CA, July 1995 **AIAA-95-2760**

NPARC Simulation and Redesign of the NASA P2 Hypersonic Inlet

Andrew Gelsey* and **Doyle D. Knight†** and **Song Gao‡** and **Mark Schwabacher§**
Rutgers, the State University of New Jersey
New Brunswick, NJ 08903

Abstract

The NPARC Reynolds-averaged Navier-Stokes code was used in a systematic redesign of the NASA P2 hypersonic inlet. The first phase of the work involved computational experiments to determine appropriate grid densities, etc. for using NPARC to achieve grid-converged simulations of the P2 inlet which adequately matched published experimental data. The second phase of the work involved formulating the redesign of the P2 inlet as a numerical optimization problem which was attacked using state-of-the-art numerical optimization software. The resulting P2 inlet design is significantly superior to the original design. In particular, the static pressure distortion at the throat was reduced by more than a factor of five.

Introduction

The P2, P8, and P12 inlets were designed in the 1970s for a proposed hypersonic cruise vehicle for Mach 10 to 12. Models were built at approximately 1/3 scale and tested in the NASA Ames 3.5 foot hypersonic wind tunnel. Extensive experimental data were gathered and reported in [Gnos *et al.* 1973]. Since then, several researchers have done two-dimensional Navier-Stokes simulations of the P2 inlet, the earliest being [Knight 1977].

The intention behind the design of these inlets was to cancel the reflected shock through surface turning at the point of impingement of the shock on the centerbody, in order to achieve high total-pressure recovery and approximately constant static pressure at the throat. The necessary surface turning was computed using the method of characteristics in conjunction with a boundary layer model. The experimental results showed that the reflected cowl shock was not canceled by the centerbody contour for any of the three inlets.

Our long-term goal for the research described in this paper is to combine Navier-Stokes simulations, numerical optimization methods, and artificial intelligence techniques to form a prototype software system which will enable the design of better inlets more rapidly and with lower cost. Our initial efforts have focused on the problem of redesigning the P2 inlet in order to successfully achieve its original design objectives, using NPARC [NASA 1994, Cooper and Sirbaugh 1989] to perform the necessary Navier-Stokes simulations. We have successfully solved this initial problem, and this paper documents the methods and experimental results we used to:

- determine appropriate grid densities, etc. for using NPARC to achieve grid-converged simulations of the P2 inlet, and compare the simulations with the experimental data of [Gnos *et al.* 1973]

- systematically modify the P2 inlet geometry to achieve very low static pressure distortion at the throat by effectively canceling the reflected shock.

NPARC input

NPARC uses the Beam-Warming approximate factorization algorithm to solve the two-dimensional[1] compressible Reynolds-averaged Navier-Stokes equations, and for our calculations turbulence was incorporated using NPARC's Chien k-ϵ model. We

* Assistant Professor, Computer Science Dept. AIAA Member.
† Professor, Dept. of Mechanical and Aerospace Engineering. AIAA Associate Fellow.
‡ Graduate Student, Computer Science Dept.
§ Graduate Student, Computer Science Dept.

[1] We are using the two-dimensional version of NPARC for the work described in this paper. A three-dimensional version of NPARC is also available.

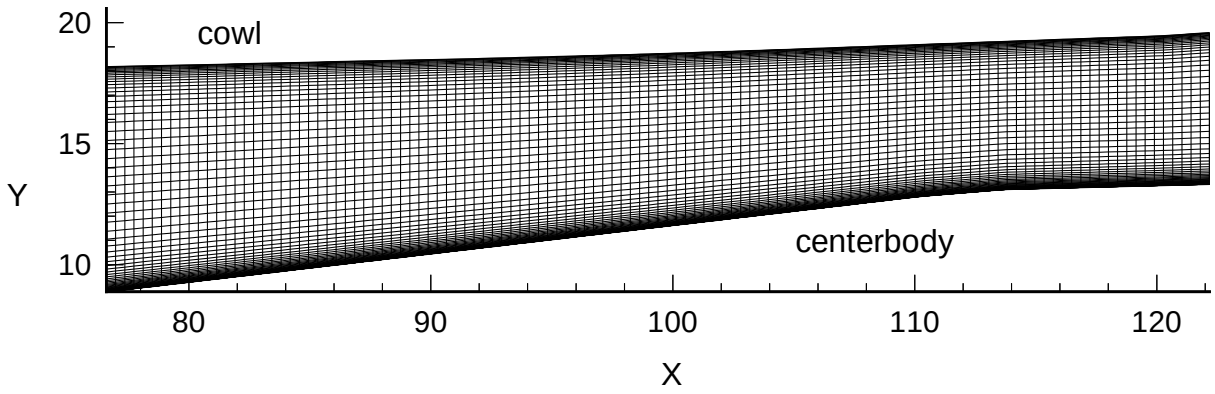

Figure 1: Standard NPARC input grid for P2 inlet (dimensions in cm)

	Standard Grid	Double Density	Quadruple Density
x points	121	241	481
y points	83	165	329
N_{BL}	46	92	183
y expansion ratio	1.15	1.0724	1.0364
$\Delta x/\delta_0$	0.380	0.190	0.0950
$\Delta y\|_{\max}/\delta_0$	0.375	0.188	0.0939
$\Delta y_2^+\|_{\mathrm{average}}$	0.153	0.0681	0.0324
cpu seconds/iteration	.97	4.8	33
iterations needed	6000	25000	25000
total compute time	1.6 hours	1.4 days	9.5 days

Legend:

N_{BL}	number of points in centerbody boundary layer
δ_0	thickness of incoming centerbody boundary layer, ≈ 1.1 cm at inlet entrance ($x = 81.28$ cm)
$\Delta y\|_{\max}$	height of grid cell with greatest y extent
Δy_2^+	nondimensional estimate of resolution of viscous sublayer on centerbody $= \dfrac{\Delta y_2 u_*}{\nu_w}$, where $u_* = \sqrt{\dfrac{\tau_w}{\rho_w}}$ and τ_w = local shear at the wall $= \mu_w \dfrac{\partial u}{\partial n}$
cpu seconds/iteration	(on Hewlett-Packard 735/125 workstation, using single precision)
iterations needed	(see Figure 3)
total compute time	(on Hewlett-Packard 735/125 workstation)

Table 1: Properties of grids used in convergence study

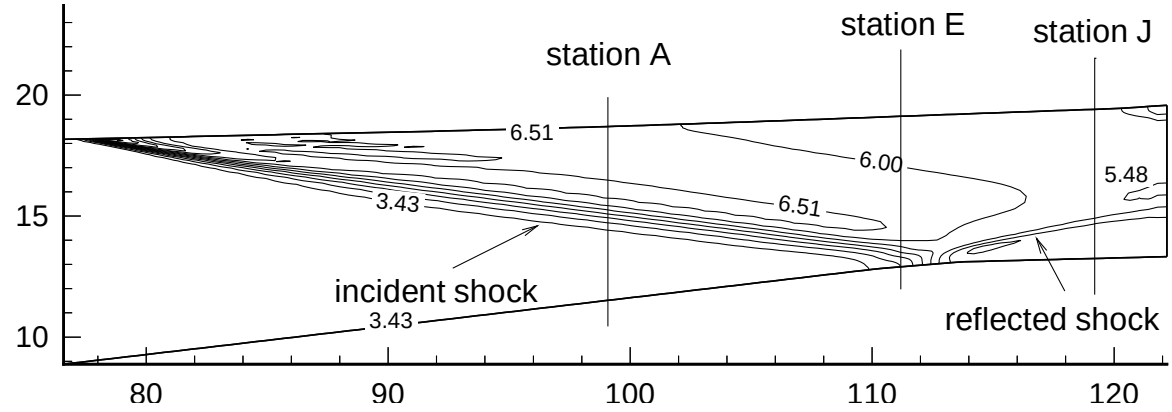

Figure 2: Pressure P/P_∞ computed by NPARC for original P2 inlet, where $P_\infty = 701.4$ Pa (freestream pressure at inlet entrance) and geometric dimensions are cm.

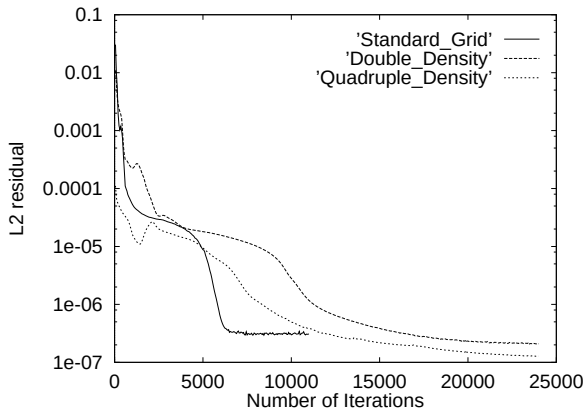

Figure 3: L2 residual as a function of iteration number (Note: restart file flow field for quadruple density case was created by interpolating partially converged flow field for double density case, so iteration numbers for quadruple density case may appear misleadingly low.)

used the following reference values in NPARC:

$$\begin{aligned} \rho_r &= 0.03602 \text{ kg/m}^3 \\ a_r &= 165.1 \text{ m/sec} \\ T_r &= 67.85^\circ \text{ K} \\ X_r &= 1 \text{ m} \end{aligned}$$

NPARC input consists of

- a restart file, which specifies a grid and a set of initial flow field values for each point in the grid, and
- a file of Fortran `NAMELIST` parameter settings.

Figure 1 shows our standard density grid, and Table 1 shows properties of each grid used in our convergence study. In constructing the grids, the shape of the inlet was taken to be the linear interpolation of the (x, y) points specified in Table 1 of [Gnos *et al.* 1973]. However, the leading edge of the cowl was extended 2.79 cm upstream in order to correctly position the shock wave generated by the cowl. This adjustment, similar to the technique employed by Knight[1977], is required since the details of the blunt-body shock in the immediate vicinity of the cowl leading edge are not resolved. Our grids use equal spacing in the x direction and exponential spacing in the y direction with an upper limit on cell growth. The experimental data of [Gnos *et al.* 1973] indicate an incoming centerbody boundary layer thickness (δ_0) of 1.1 cm, and Table 1 shows that the number of points our grids have in this centerbody boundary layer compares favorably with the 30 points suggested by the traditional rule of thumb. Table 1 also gives values of $\Delta y_2^+|_{\text{average}}$ computed from our converged NPARC solutions, indicating an adequate resolution of the viscous sublayer on the centerbody.

We used the Chien k-ϵ model in the EDDYBL turbulent boundary layer code [Wilcox 1993] to generate a flow field profile immediately upstream of the inlet which matched the experimental conditions. The freestream conditions at the entrance to the inlet are

$$\begin{aligned} M &= 5.8 \\ p_{t_0} &= 2.6910^6 Pa \\ T_{t_0} &= 770^\circ \ K \end{aligned}$$

and the incoming centerbody boundary layer thickness $\delta_0 = 1.1$ cm. This profile was used as the fixed upstream boundary condition for NPARC and was also propagated throughout the domain to give an initial flow field for the NPARC computation.

The appendix of this paper includes a verbatim copy of the Fortran `NAMELIST` parameter settings for NPARC used with our standard grid. The only changes for the other grids were those required because of the increased number of grid points. We used a fixed upstream boundary condition with the flow field computed as described above. The walls of the P2 inlet were cooled as described in [Gnos *et al.* 1973], so we used the no-slip isothermal boundary condition. Finally, we used the extrapolation boundary condition for the downstream boundary and for the section between the upstream boundary and the cowl.

We used NPARC default values for most other NPARC parameters, though we did change two smoothing parameters. (The appendix includes data on the effects of NPARC smoothing parameters.) We also reduced the local Courant number `DTCAP`.

Results of convergence study

The pressure contours in Figure 2 show the incident and reflected shock in the original P2 inlet. Figure 4 shows both the experimentally measured pitot pressure at $x = 99.06$ cm, and the pitot pressure as computed by NPARC using the grids listed in Table 1, normalized by the upstream freestream total pressure $p_{t_\infty} = 4.14\ 10^6$ Pa. The standard grid clearly does not yield a grid-converged solution. NPARC uses a second-order accurate algorithm, so doubling grid density should theoretically reduce error by a factor of four; our computational data appears to roughly match this theoretical prediction. Given

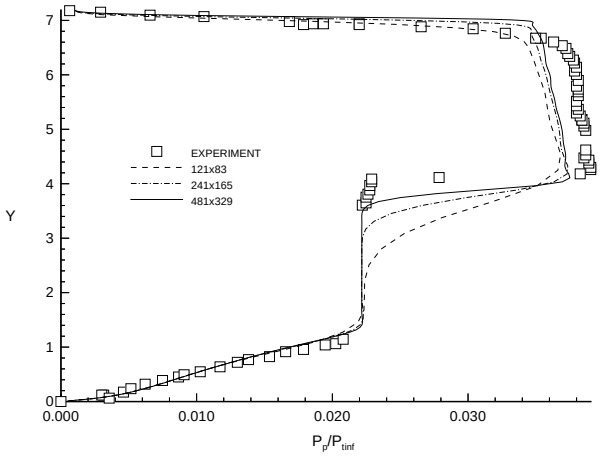

Figure 4: Pitot pressure at station A (x = 99.06 cm), normalized by upstream freestream total pressure p_{t_∞} = 4.14 10^6 Pa. (Y axis shows cm measured vertically from centerbody. Experimental data is from Figure 36a of [Gnos *et al.* 1973].)

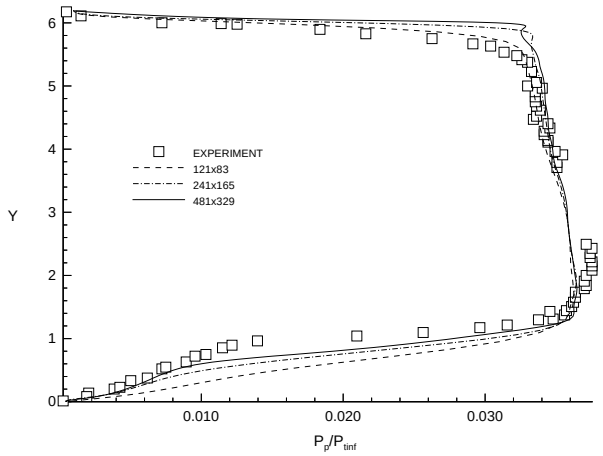

Figure 5: Pitot pressure at station E (x = 111.76 cm), normalized by upstream freestream total pressure p_{t_∞} = 4.14 10^6 Pa. (Y axis shows cm measured vertically from centerbody. Experimental data is from Figure 36e of [Gnos *et al.* 1973].)

this convergence rate, the results with the double density and quadruple density grid are sufficiently close together that it seems likely that our quadruple density grid approximates a grid-converged solution to the level of accuracy of the experimental data (i.e., typically one to three percent, depending on the quantity [Gnos et al 1973]).

Figures 5 and 6 show the experimental and computational pitot pressure at stations farther downstream, and Figures 7 and 8 shows experimental and computational surface pressure distributions. In all cases NPARC's grid convergence behavior seems roughly second-order, which is consistent with the theoretical convergence rate for the algorithm. The computations using the quadruple density grid seem to give a good match to the experimental data for most of the flow field, though there are a few areas of discrepancy which merit further investigation. In Figure 6 note the reflected shock at y $\approx$ 1 cm: below we discuss our methods for redesigning the inlet to eliminate this reflected shock. The reflected shock in the double density and quadruple density grids is fairly close to the experimental data; the reflected shock in the standard grid does not match the experimental data quite as well, but it is still quite pronounced.

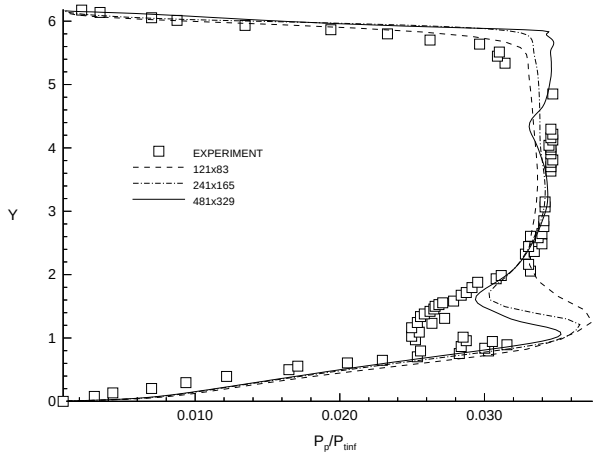

Figure 6: Pitot pressure at station J (x = 119.38 cm), normalized by upstream freestream total pressure p_{t_∞} = 4.14 10^6 Pa. (Y axis shows cm measured vertically from centerbody. Experimental data is from Figure 36j of [Gnos *et al.* 1973].)

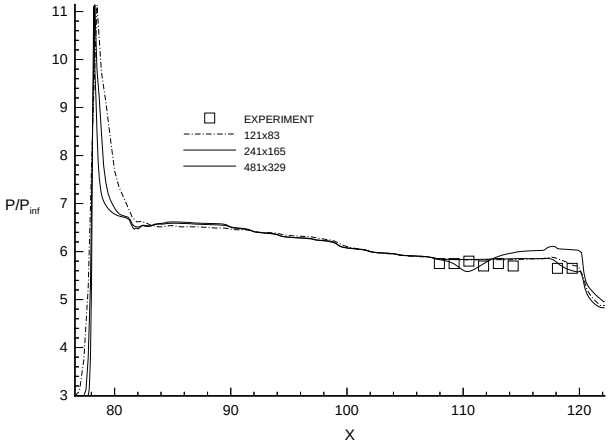

Figure 7: Surface pressure distribution on cowl, P/P_∞ where $P_\infty = 701.4$ Pa, freestream pressure at inlet entrance. (X axis in cm, experimental data from Figure 31 of [Gnos *et al.* 1973].)

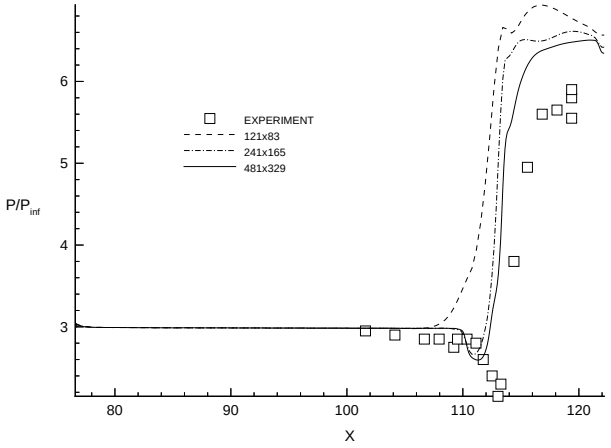

Figure 8: Surface pressure distribution on centerbody, P/P_∞ where $P_\infty = 701.4$ Pa, freestream pressure at inlet entrance. (X axis in cm, experimental data from Figure 31 of [Gnos *et al.* 1973].)

Redesign of the P2 inlet

We used four measures of merit to evaluate candidate inlet designs[2]:

1. static pressure distortion at the throat, defined by
$$\sigma_p \equiv \frac{1}{\bar{p}} \left\{ \frac{1}{H} \int_0^H (p - \bar{p})^2 dy' \right\}^{1/2}$$
where $\bar{p}$ is the mean static pressure at the throat
$$\bar{p} \equiv \frac{1}{H} \int_0^H p \, dy',$$
H is the height of the throat, and y' is measured (vertically) from the lower surface
2. mean static pressure recovery, defined by
$$r_p \equiv \frac{1}{H p_\infty} \int_0^H p \, dy'$$
where p_∞ is the static pressure immediately upstream of the inlet entrance
3. total pressure distortion at the throat, defined by
$$\sigma_{p_t} \equiv \frac{1}{\bar{p_t}} \left\{ \frac{1}{H} \int_0^H (p_t - \bar{p_t})^2 dy' \right\}^{1/2}$$
where $\bar{p_t}$ is the mean total pressure at the throat
$$\bar{p_t} \equiv \frac{1}{H} \int_0^H p_t \, dy'$$
4. mean relative total pressure at the throat, defined by
$$r_{p_t} \equiv \frac{1}{H p_{t_\infty}} \int_0^H p_t \, dy'$$
where p_{t_∞} is the upstream freestream total pressure measured in the freestream flow at the entrance to the inlet

Table 2 shows the values of these measures of merit computed for the original P2 inlet. The mean static pressure recovery r_p, the total pressure distortion at the throat σ_{p_t}, and the mean relative total pressure r_{p_t} at the throat manifest quadratic convergence, *i.e.*, the relative change from the double to quadruple grid is typically a factor of four less than the relative change from the single to the double. The static pressure distortion σ_p displays an approximate 4%-5% variation between successive grid refinements. This relatively constant variation is attributable to the emergence of successively weaker waves in the inlet flowfield as the grid

[2] All quantities are evaluated at the at the nominal throat (station J, $x = 119.38$ cm)

		Standard	Double	Quadruple
σ_p	(S)	0.069858	0.072820	0.07616
	(D)	0.069856	0.072819	0.07614
r_p	(S)	2.00528	1.9514	1.9403
	(D)	2.00531	1.9514	1.9413
σ_{p_t}	(S)	0.3942	0.3774	0.3828
	(D)	0.3942	0.3775	0.3832
r_{p_t}	(S)	0.4957	0.5163	0.5189
	(D)	0.4957	0.5163	0.5187

Legend:
(S) Computation using single precision (32 bit)
(D) Computation using double precision (64 bit)

Table 2: Measures of merit for original P2 inlet computed using standard, double density, and quadruple density grids

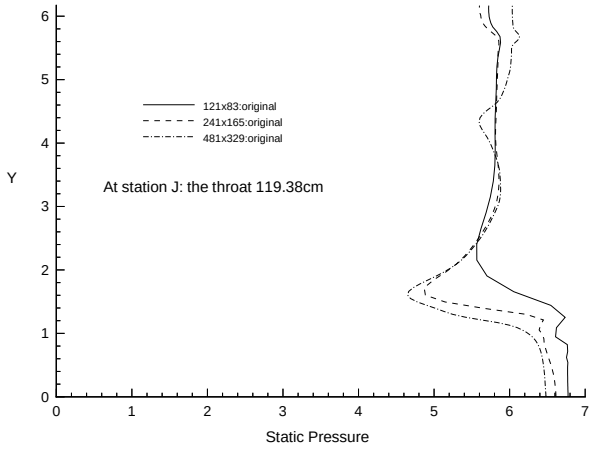

Figure 9: Static pressure profile at the nominal throat (station J, $x = 119.38$ cm) for the original P2 inlet as computed by NPARC with standard grid, double density grid, and quadruple density grid; P/P_∞ where $P_\infty = 701.4$ Pa, freestream pressure at inlet entrance. (Y axis shows cm measured vertically from centerbody.)

is refined. As indicated in Figure 9, however, the static pressure profile at the throat for the double and quadruple cases are virtually identical; in particular, the structure of the reflected shock (at y $\approx$ 1 cm) is very similar for both grids. We therefore conclude that the uncertainty in the numerical prediction of the static pressure distortion is no more than 10%. Also, note single precision (32 bit) and double precision (64 bit) gave effectively identical results for these calculations.

Our systematic redesign of the P2 inlet consisted of two steps:

1. Define a parameterized space of candidate P2 redesigns

2. Systematically search the space of candidate P2 redesigns using a numerical optimization method

All inlets in our parameterized space of candidate P2 redesigns used the same cowl contour as the original P2 inlet. For redesign, we discarded the original P2 centerbody contour and instead used a parameterized contour consisting of three sections, as shown in Figure 10. The left section is a straight line rising at angle θ which terminates at point (x_l, y_l). The right section is a straight line turned through angle $\Delta\theta$ relative to the left line, starting at a point offset by $(\Delta x, \Delta y)$ from the end of the left section. The middle section is a smooth curve whose shape is uniquely determined by the requirement that it connect the left and right sections and match their slopes. This smooth curve is parametrically generated as follows:

$$\begin{pmatrix} x \\ y \end{pmatrix} = \begin{pmatrix} x_c \cos p + x_s \sin p + x_0 \\ y_c \cos p + y_s \sin p + y_0 \end{pmatrix}, \; 0 \le p \le \frac{\pi}{2}$$

and the six coefficients are uniquely[3] determined by the following six requirements:

p	$x(p)$	$y(p)$	angle
0	x_l	y_l	θ
$\pi/2$	$x_l + \Delta x$	$y_l + \Delta y$	$\theta + \Delta\theta$

The centerbody contour for our redesigned P2 inlet is mathematically defined to be the portion of this parameterized contour which lies between the upstream boundary (76.59 cm) and the downstream boundary (122.18 cm) of our NPARC computational domain. This mathematical definition does not require that the portion of the parameterized contour within the computational domain must include all three sections of the full parameterized curve shown in Figure 10.

[3] except in the case $\Delta\theta = 0$

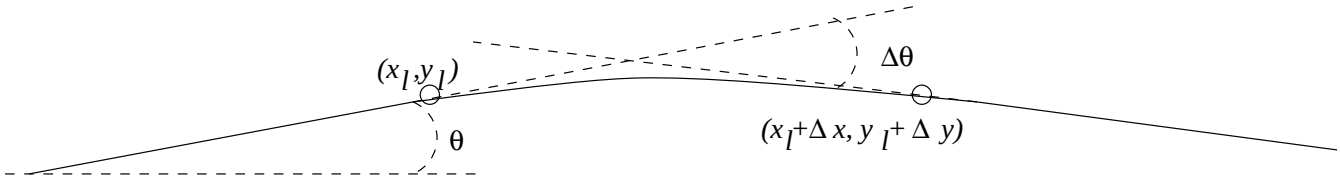

Figure 10: Parameterized contour for redesign of P2 inlet centerbody

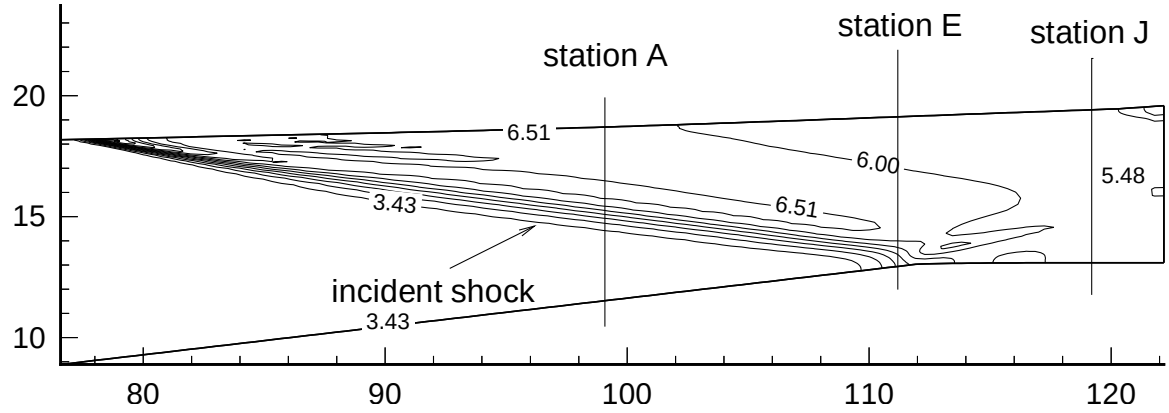

Figure 11: Pressure P/P_∞ computed by NPARC for optimal redesigned P2 inlet, where P_∞ = 701.4 Pa (freestream pressure at inlet entrance) and geometric dimensions are cm.

To find an optimal redesign of the P2 inlet, we automatically searched our space of candidate designs using CFSQP, a state-of-the-art implementation of the sequential quadratic programming method [Craig *et al.* 1994]. The appendix includes a brief overview of nonlinear optimization, sequential quadratic programming, and CFSQP.

In our systematic redesign of the P2 inlet, we attempted to minimize the first measure of merit, static pressure distortion σ_p at the inlet throat. We also imposed loose constraints on r_p, the mean static pressure recovery.[4] The other two measures of merit were allowed to vary freely, but monitored to ensure that improvements in static pressure distortion did not require significant sacrifices in quality of the other measures of merit.

We configured CFSQP to minimize static pressure distortion by simultaneously varying the four parameters x_l, Δx, Δy, and $\Delta\theta$ in Figure 10. Therefore we had a four-dimensional space of candidate inlet designs to search through in order to find an optimal design. All NPARC runs during the numerical optimization were done in single precision with our standard grid. CFSQP was not allowed to vary two remaining parameters: θ was fixed and y_l

[4]However, these constraints were not active at the optimal design we found.

x_l	=	111.89 cm
y_l	=	13.02 cm
θ	=	0.1167 radians
Δx	=	47.05 cm
Δy	=	-0.13 cm
$\Delta\theta$	=	0.1249 radians

Table 3: Design parameters for optimal redesigned P2 inlet

Measure	Original	Optimal	Change
σ_p	0.0699	0.0134	$-\mathbf{80.1}\%$
r_p	2.0053	1.9238	-4.1%
σ_{p_t}	0.3942	0.4014	1.8%
r_{p_t}	0.4957	0.4926	0.6%

Table 4: Measures of merit for original P2 inlet and best redesigned P2 inlet (both computed with standard density grid)

was computed as

$$y_l = x_l \tan\theta + y_0$$

The constant values for θ and y_0 were chosen to make the ramp (left section) of the redesigned centerbody coincide as closely as possible with the ramp of the original P2 inlet.

Figure 11 shows the pressure contours for the best redesigned P2 inlet found by CFSQP. Note

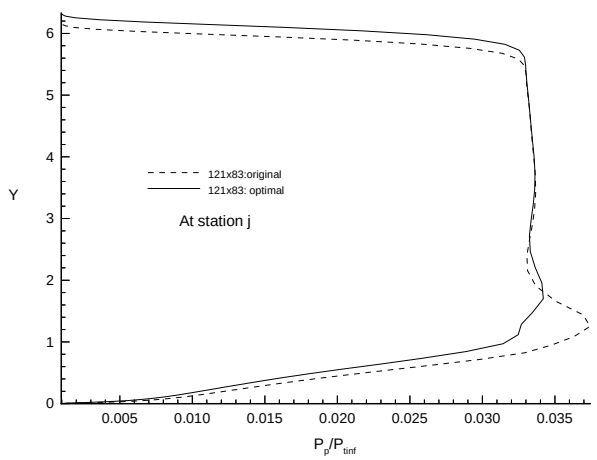

Figure 12: Pitot pressure at station J, x = 119.38 cm for original and optimized P2 inlets. (Normalized by upstream freestream total pressure p_{t_∞} = 4.14 10^6 Pa. Y axis shows cm measured vertically from centerbody.)

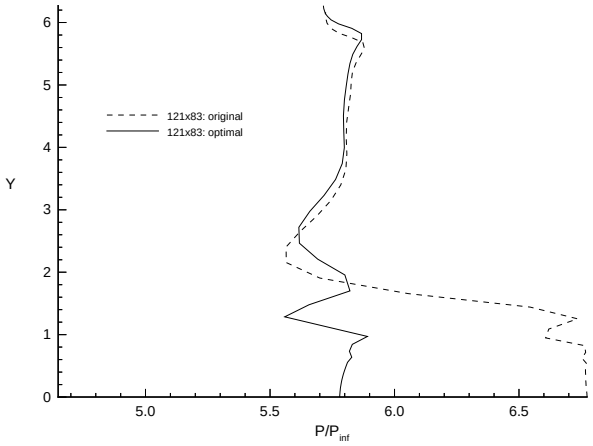

Figure 14: Static pressure profile at the nominal throat (station J, x = 119.38 cm) for original and optimized P2 inlets, P/P_∞ where P_∞ = 701.4 Pa, freestream pressure at inlet entrance. (Y axis shows cm measured vertically from centerbody.)

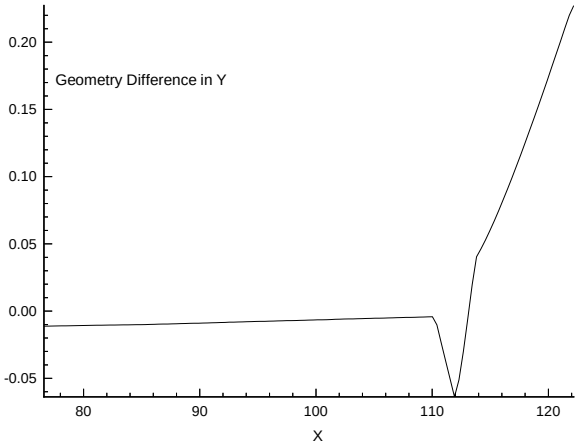

Figure 13: Centerbody y(original) - y(optimal) as a function of x (dimensions in cm)

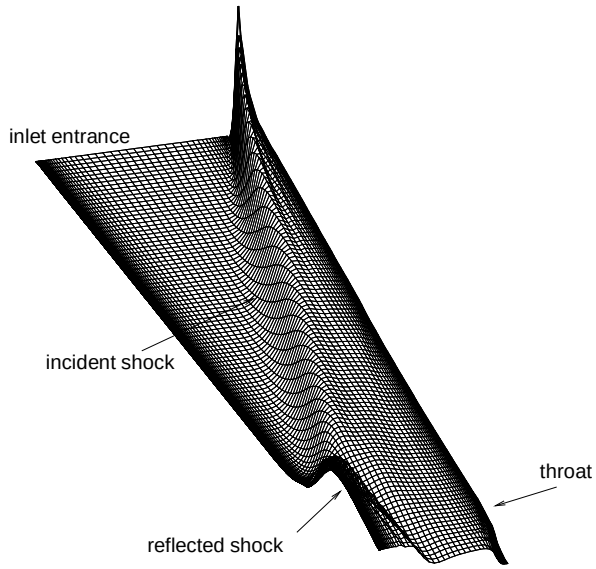

Figure 15: "3D" version of Figure 2, static pressure in original P2 inlet

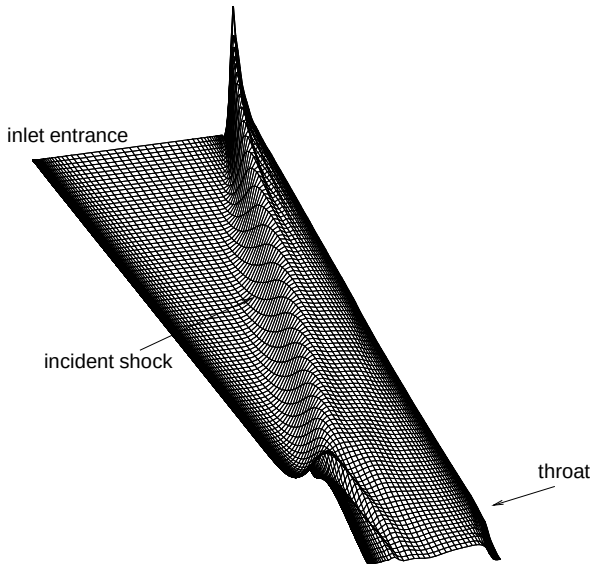

Figure 16: "3D" version of Figure 11, static pressure in optimal redesigned P2 inlet

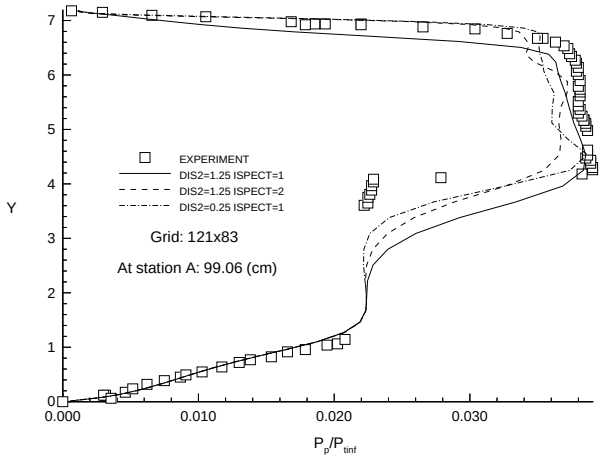

Figure 17: Effect of NPARC smoothing parameters on pitot pressure (normalized by upstream freestream total pressure $p_{t_\infty} = 4.14\ 10^6$ Pa) at $x = 99.06$ cm.

that the reflected shock has been virtually eliminated, as desired. This cancellation can also be seen in Figure 12, which compares the pitot pressure at $x = 119.38$ cm for the original and optimized P2 inlets. Figures 15 and 16 show "3D" versions of the pressure distributions for the original and optimized P2 inlets which more vividly illustrate the cancellation of the reflected shock. The design parameters for this optimal redesigned P2 inlet are shown in Table 3 and the resulting measures of merit are shown in Table 4. Note that the point $x_l + \Delta x$ is past the downstream boundary (122.18 cm) of our NPARC computational domain, as is allowed by our mathematical definition of the centerbody contour for our redesigned P2 inlet given above.

Comparison with the measures of merit for the original P2 inlet shown in Table 2 shows that static pressure distortion has been greatly reduced by more than a factor of five. The other three measures of merit are unchanged from the values for the original P2 inlet, to within experimental and numerical truncation errors for the data. Figure 13 shows the difference in y as a function of x between the original and optimal inlets. Figure 14 shows the static pressure profiles at the throat for the two inlets. To find this optimum, CFSQP used NPARC to evaluate approximately 60 candidate inlet designs. Based on the Table 1 timing data, about four days are required for a complete optimization on a Hewlett-Packard 735/125 workstation. We are presently investigating how sensitive the solution quality and search time are to the choice of the initial design at which the search starts.

Conclusion

We have shown:

- NPARC can successfully compute a grid-converged simulation of the P2 inlet which is a good match with experimental wind tunnel results.
- Redesign of the P2 inlet can be formulated as a numerical optimization problem, and solving that problem leads to a significantly superior P2 inlet design. In particular, the static pressure distortion at the throat was reduced by more than a factor of five.

Appendix

NPARC Smoothing parameters

An extensive parameter study was performed to ascertain the sensitivity of the computed solution to three parameters `ISPECT`, `DIS2` and `DIS4`. These parameters control the nature and level of the numerical smoothing.

The recommended (default) values for `DIS2` (0.25), `DIS4` (0.64) and `ISPECT` (2) were found to be inadequate. As indicated in Figure 17, significant oscillations were observed downstream of the cowl shock wave. Increasing `DIS2` to 1.25 and changing `ISPECT` to 1 was found necessary to eliminate the

oscillations. Similar changes in DIS4 were found to have minimal effect on the computed solution. Variations in the three parameters had a negligible effect on the centerbody boundary layer (Figure 17).

Fortran NAMELIST parameter settings

```
$INPUTS
  RE        = 1.30184e+06,
  PR        = 0.72,
  PREF      = 701.4,
  TREFR     = 122.13,
  TSUTH     = 198.6,
  VRAT      = -0.66667,
  XMACH     = 7.4,
  ALPHA     = 0.0,
  IAXISY    = 0,
  NBLOCK    = 1,
  ISOLVE    = 1,
  NMAX      = 8000,
  IVARDT    = 2,
  DTCAP     = 0.75,
  PCQMAX    = 10.0,
  NUMDT     = 0,
  IMASS     = 1,
  POSD      = 2116.53,
  TOSD      = 518.4,
  NC        = -1,
  STOPL2    = 1.E-11,
  STOPTR    = 100.,
  DIS2      = 1.25,
  DIS4      = 0.64,
  IFILTR    = 1,
  ISPECT    = 1,
  SPLEND    = 1,
  SMOO      = 0.0,
  NP        = 501,
  NSPRT     = 50,
  IFXPRT    = 0,
  IPLOT     = 0,
  L2PLOT    = 0,
  IFXPLT    = 1
$END
$TURBIN
  PRT       = 0.9,
  IMUTUR    = 2,
  ITCOMP    = 0,
  IFMAX     = 3,
  NTURB     = -1000,
  NRLX      = 1,
  ORDER     = 1.0,
  TMUMAX    = 10000.,
  UREFKE    = 5.0
$END
$BLOCK
  INVISC(1) = 1,
  INVISC(2) = 1,
  LAMIN(1)  = 0,
  LAMIN(2)  = 1,
  DTBLK     = 0.0,
  DIS2      = 1.25,
  DIS4      = 0.64,
  GAMMA     = 1.4,
  COFMIX    = 0.09,
  NBCSEG    = 0,
  NPSEG     = 0
$END
$BOUNDS
  NJSEG         = 2,
    JLINE(1)    = 1,
      JKLOW(1)  = 1,
      JKHIGH(1) = 83,
      JSIGN(1)  = 1,
      JTYPE(1)  = -10,
    JLINE(2)    = 121,
      JKLOW(2)  = 1,
      JKHIGH(2) = 83,
      JSIGN(2)  = -1,
      JTYPE(2)  = 3,
  NKSEG         = 3,
    KLINE(1)    = 1,
      KJLOW(1)  = 2,
      KJHIGH(1) = 120,
      KSIGN(1)  = 1,
      KTYPE(1)  = 61,
      TEMPK(1)  = 4.6,
    KLINE(2) = 83,
      KJLOW(2)  = 2,
      KJHIGH(2) = 5,
      KSIGN(2)  = -1,
      KTYPE(2)  = 3,
    KLINE(3) = 83,
      KJLOW(3)  = 6,
      KJHIGH(3) = 120,
      KSIGN(3)  = -1,
      KTYPE(3)  = 61,
      TEMPK(3)  = 4.4,
$END
```

Nonlinear Optimization

A *nonlinear programming* [Vanderplaats 1984, Moré and Wright 1993, Gill *et al.* 1981] problem consists of a nonlinear *objective function* to be minimized, and a set of nonlinear *constraints*. It can be expressed as

$$\min f(\mathbf{x}) \tag{1}$$

$$\text{s.t. } \mathbf{g}(\mathbf{x}) \leq \mathbf{0} \tag{2}$$

where $\mathbf{x}$ is a vector, representing the variables, f is a scalar function, representing the objective function, and $\mathbf{g}$ is a vector function, representing the constraints.

A *quadratic programming* problem is a special case of a nonlinear programming problem in which the objective function f is quadratic, and the constraint function $\mathbf{g}$ is linear. The *sequential quadratic programming* (SQP) method solves a nonlinear programming problem by solving a sequence of quadratic programming problems as follows:

1. fit a quadratic program to the nonlinear program
2. solve the quadratic programming problem
3. perform a minimization along the line defined by the current point and the minimum of the quadratic programming problem
4. repeat

Fitting a quadratic program to the objective function can be done by computing the Hessian of the objective function f with respect to $\mathbf{x}$, and the gradient of each constraint function g_i with respect to $\mathbf{x}$. Since computing the Hessian is expensive, an approximation of the inverse of the Hessian, known as the *quasi inverse Hessian*, is used. The quasi inverse Hessian is updated on each iteration using the gradient of f with respect to $\mathbf{x}$. In CFSQP, this update is done using the Broyden-Fletcher-Goldfarb-Shanno update formula. SQP is thus a *quasi-Newton* method.

Solving a quadratic programming problem is a much easier task than solving an arbitrary nonlinear programming problem. CFSQP uses the package QLD, an implementation of Powell's method of solving quadratic programming problems, to solve the quadratic programming problem at each iteration.

CFSQP terminates when one of two conditions is met. The first condition is that the Kuhn-Tucker vector is within a certain tolerance of zero. This means, roughly, that the objective function gradient vector and the gradient vectors of the active constraint functions are pointing in opposite directions. The second condition is that the improvement in the objective function during the line minimization is less than a certain tolerance.

Acknowledgments

This research is part of the HPCD (Hypercomputing and Design) project based at Rutgers University and has involved collaboration with Vijay Shukla of the Rutgers Department of Mechanical and Aerospace Engineering and Don Smith and Tom Ellman of the Rutgers Computer Science Department. We have had very helpful discussions about inlet design with David Sobel and Marty Haas (United Technologies Research Center) and Gerald Paynter (Boeing Commercial Aircraft Co.). The HPCD project is supported by the Advanced Research Projects Agency of the Department of Defense through contract ARPA-DABT 63-93-C-0064. The contents of this paper do not necessarily reflect the position of the United States government and official endorsement should not be inferred.

References

G. K. Cooper and J. R. Sirbaugh. PARC code: Theory and usage. Technical Report AEDC-TR-89-15, Arnold Engineering Development Center, Arnold Air Force Base, Tennessee, December 1989.

L. Craig, J. Zhou, and A. Tits. User's guide for CFSQP version 2.1: A C code for solving (large scale) constrained nonlinear (minimax) optimization problems, generating iterates satisfying all inequality constraints. Technical Report TR-94-16r1, Institute for Systems Research, University of Maryland, November 1994.

Philip E. Gill, Walter Murray, and Margaret H. Wright. *Practical Optimization.* Academic Press, London ; New York, 1981.

A. Vernon Gnos, Earl C. Watson, William R. Seebaugh, Robert J. Sanator, and Joseph P. DeCarlo. Investigation of flow fields within large-scale hypersonic inlet models. Technical Report TN D-7150, NASA, April 1973.

Doyle D. Knight. Numerical simulation of realistic high-speed inlets using the Navier-Stokes equations. *AIAA Journal*, 15(11):1583–1589, 1977.

Jorge J. Moré and Stephen J. Wright. *Optimization Software Guide.* SIAM, Philadelphia, 1993.

NASA. NPARC 1.2a user notes. Technical report, NASA, July 1994.

Garret N. Vanderplaats. *Numerical Optimization Techniques for Engineering Design : With Applications.* McGraw-Hill, New York, 1984.

David C. Wilcox. *Turbulence Modeling for CFD.* DCW Industries, Inc., La Cañada, California, 1993.